Grau Meló, R.; Verdú, S.; Pérez Jiménez, AJ.; Barat Baviera, JM.; Talens Oliag, P. (2021). Laser-backscattering imaging for characterizing pork loin tenderness. Effect of pre-treatment with enzyme and cooking. Journal of Food Engineering. 299:1-8. https://doi.org/10.1016/j.jfoodeng.2021.110508

Laser-backscattering imaging for characterizing pork loin tenderness. Effect of pre-treatment with enzyme and cooking

[1]Raúl Grau, [1]Samuel Verdú, [2]Alberto J. Pérez, [1]José M. Barat, [1]Pau Talens,

[1]Departamento de Tecnología de Alimentos. Universitat Politècnica de València, Spain

[2]Departamento de Informática de Sistemas y Computadores, Universitat Politècnica de València, Spain

*Author for correspondence: Raúl Grau

Address: Edificio 8E - Acceso F – Planta 0

Ciudad Politécnica de la Innovación

Universitat Politècnica de València

Camino de Vera, s/n

46022 VALENCIA – SPAIN

E-mail: rgraume@tal.upv.es

Abstract

The aim of this work was to characterizes, by the non-destructive technique based on the laser-backscattering imaging analysis, the effect of pre-treatment with papain enzyme (1% w/w), the enzyme action time (0, 3, 6 and 24 h at 4 ºC) and cooking (80 ºC for 3 min) on pork loin tenderness. Texture and image analyses were run for the untreated and treated samples, and for the uncooked and cooked samples. Images of the laser pattern generated on the meat surface were decomposed into red, green and blue channels. Two descriptors types (direct and relative) were developed for each one by segmentation. The obtained results revealed the increased tenderness in the samples that underwent enzyme treatment with maximum values at 6 h (29.3±3.2 N). Cooking increased enzyme action with much lower values (39.2±3 N) than for the samples without treatment (75.6±2.9 N). For uncooked meat, changes in texture were related mainly to the relative descriptor of the blue and green channels, and those from the red channel for cooked meat, which allowed prediction models to be obtained (R^2 CV = 0.9; RMSE CV = 1.9).

Keywords: meat softness, papain, diffuse reflectance, biospeckle, non-destructive analysis

1. Introduction

Tenderness is one of the most important meat characteristics (Bhat et al., 2018; Lomiwes et al., 2014; Takei et al., 2015), and is described as the most important factor to influence consumer satisfaction (Bolumar et al., 2014; Silva et al., 2015). Ageing is an effective traditional way to improve tenderness and other meat characteristics (Bhat et al., 2018). Meat proteins are known to undergo intense degradation during postmortem ageing due to the action of calpains and cathepsins, which results in increased meat tenderness (Toldrá, 2012). The main changes are associated with myofibrils fragmentation through the Z-disc, the degradation of desmin, titin and nebulin, and the appearance of two polypeptides with molecular masses of 95 and 30 KDa (Toldrá and Reig, 2015).

Increasing meat tenderness and flavour is often done by ageing it, but this involves economic considerations in time, space, labour and energy terms (Bhat et al., 2018). In addition, tenderization by ageing is limited and sometimes proves insufficient for certain population sectors that can only eat very soft food. In fact with decreased chewing function due to prosthesis placement and muscle weakness associated with ageing, or sequelae of stroke or other diseases/injuries, people like the elderly can become increasingly unable to eat meat, which is very tasty food, and serves as a good protein source that comes in normally cooked dishes. This may lead to protein deficiencies in this population (Takei et al., 2015). However, the problem can increase because the cooking process sometimes increases meat toughness. In muscles in which myofibrillar proteins predominate, such as *Longissumus lumborum*, a high temperature rate is applied, and the denaturation of myofibrillar components results in toughening (Walsh et al., 2010).

To increase meat tenderness, other strategies like chemical and mechanical methods are adopted. Chemical methods include post-exsanguination vascular infusion and exogenous proteases, solubilising agents likes salt (marination) and calcium. Mechanical

methods consist in grinding, blade or needle tenderisation and applying high-pressure processing (HPP) pre- or post-rigour in combination with or without heat (Bolumar et al., 2014). Applying enzymes for meat tenderisation has been considered for years. Exogenous protease enzymes, such as papain, bromelain and ficin, are widely used as meat tenderizers (Eom et al., 2015; Takei et al., 2015; Toldrá and Reig, 2015). Papain is extracted from papaya latex (EC 3.4.22.2) and is one of the commonest plant enzymes employed for artificial meat tenderisation because of its ability to break down both myofibrillar proteins and connective tissues (Barekat and Soltanizadeh, 2017). In these studies, softness is evaluated with mechanical properties by employing a texturometer, which very well describes the texture of meat, but in a destructive analysis. So when samples need to be measured at different times during their transformation, it is say, at the same time that they are undergoing changes, heterogeneity must be assumed among them or their number should increase during each sampling time. Recently, imaging methods have been utilised to visually assess meat and foodstuff quality of the processing line based on colour, shape, size, surface texture features, etc. Technically speaking, image processing is a methodology capable of offering an accurate physical description of an object through image analysis (Taheri-Garavand et al., 2019) without destroying it.

Among other imaging techniques, the laser backscattering method has also been applied to model and characterize food properties, and for processing both solid and fluid food matrices. This approach is based on a simple device, which also includes image analysis procedures, from which the interaction of laser with samples is captured on digital images as diffraction patterns. In this approach, the laser is transmitted through the matrix until the surface and is scattered because of the sample's internal structure and components. Light scattering is the result of photon projection at different angles in a given material. Hence of the total laser light projected onto the food surface, a fraction of photons is

92 reflected on it, while the rest enter food tissue and undergoes absorption (related to the
93 chemical constituents), transmission, or diffuse reflection (scattering) (Udomkun et al.,
94 2014). These phenomena may provide information about the structures and morphology
95 of the matrix because the backscattered photons have inherently interacted with the
96 internal components (Mollazade et al., 2013).

97 The patterns from these digital images are processed and transformed into numerical data,
98 which can be used to predict food and process parameters for non-destructive
99 physicochemical monitoring. One of the main advantages of this technique, apart from
100 its low cost, is it can be applied to study static or dynamic samples, which change as they
101 are being measured. Recently, our research group successfully worked with this technique
102 by applying it to evaluate the rheological properties of vegetable-based creams (Verdú et
103 al., 2019c), the physico-chemical properties of biscuits with different fibre contents
104 (Verdú et al., 2019a) and by monitoring the texture of milk during fermentation for yogurt
105 production (Verdú et al., 2019b) or cheese curing (Verdú et al., 2020).

106 Thus, the aim of this work is to characterize, by the non-destructive technique based on
107 the laser-backscattering imaging analysis, the effect of the pre-treatment with papain
108 enzyme, the enzyme action time and cooking, on pork loin tenderness.

109

110 **2. Material and Methods**

111 2.1. Experimental design

112 This study was carried out with sliced fresh pork loins (*Longissumus dorsi*) (7 mm
113 thickness), purchased from a local Spanish supermarket (Mercadona, Spain). Samples
114 were repackaged in plastic bags by mixing slices from different lots to reduce the batch
115 effect.

116 Three factors were studied: enzyme treatment, enzyme action time and cooking process.
117 For this purpose, 96 samples were employed, half of which were treated with the enzyme,
118 and the remaining 48 were used as the control. The enzyme was papain (Biocon, Les
119 Franqueses del Vallés, Spain), a proteolitic enzyme (Singh et al., 2018) with an activity
120 of 6000 USP. Firstly, 1% (w/w), which is the least amount capable of covering the entire
121 surface, was directly applied to the surface of the sliced loins, which were kept at 4 ºC
122 during the enzyme action time (0, 3, 6 and 24 h) on a Petri dish. For each time, half the
123 control and treated samples were placed individually inside plastic bags and cooked at 80
124 ºC for 3 min, while the rest were analyzed without heat treatment (Fig. 1B). The cooking
125 method was chosen to obtain homogeneous heat diffusion around samples, without
126 allowing the cooking liquid to interact with samples. Later at room temperature, the
127 samples that had undergone enzyme treatment and the control ones (without it) were
128 analyzed at each enzyme action time, either with or without heat treatment (12 samples
129 each). The mass variation, texture, image analysis and correlation between them were
130 noted to describe the changes that took place according to the factors. Fig. 1B shows the
131 experimental design.

132

133 2.2. Physical properties

134 2.2.1. Texture analysis

135 For all the samples, texture was analyzed at each sampling time and room temperature by
136 employing the slice shear force (SSF) according to that described by Bruce and Aalhus
137 in 2017. A TA-XT2 texture analyser (Stable Microsystems, England) was used and the
138 crosshead speed was set at 500 mm/min. The blade employed for shearing was flat with
139 a similar degree of bevel (half-round) and thickness (1.684 mm). The software was

140 Exponent (Stable Micro Systems Ltd, version 6.1.11.0), and shear force was obtained and
141 expressed as Newton (N).

142 2.2.2. Mass loss

143 All the samples were weighed at time 0 and after each enzymatic action time (3, 6 and 24
144 h), as were the cooked ones later. By employing Equation 1, the mass loss for each
145 enzyme action time, because of the cooking process, was calculated.

146

147 $\Delta M = \frac{(mf - mo)}{mo}$ (1)

148 where ΔM is the mass increment for the enzyme action time; mf is mass after each enzyme
149 action time; mo is the initial mass. For the cooking process action: mf is the mass after
150 cooking and mo is the mass at the end of each enzyme action time.

151

152 2.2.3. Imaging system and descriptors

153 The imaging system was based on capturing the generated laser backscattering pattern
154 onto the loin surface because of the light transmitted from the bottom of the sample. The
155 capture system was a Logitech C920 camera (CMOS sensor, resolution of 2304x1535)
156 placed inside a dark cabin to keep it away from light, and 15 cm vertically over the sample
157 surface. It was placed in the middle of the capture field. The laser pointer (650 nm,
158 50 mW, 3 mm⌀) was perpendicularly placed 9 cm under samples by emitting to the
159 central zone of the bottom surface (Fig. 1A). The selected laser specifications were
160 decided according to previous studies, where one red light-laser pointer was successfully
161 used (Tu et al., 2000; Verdú et al., 2019a). In this case, power was higher to obtain a
162 sufficient transmittable light fraction because of the properties of the studied food matrix.

163 The RGB (red, green and blue) images (1280 × 720 pixels in the JPEG format) were
164 captured for each sample type, employing version 2.51 of Logitech Webcam Software
165 (compilation 13.51.828). All automatic light controls parameters were set to manual mode
166 in order to work with consistent light captures (gain, shutter speed, white balance, …).

167 Image descriptors were extracted following the steps shown in Fig. 1C and 1D and in the
168 Supplementary Material (Fig. 1): firstly, the RGB images were cut to 350 x 350 pixels,
169 and then the fraction of each different image from the samples was removed to avoid
170 reflections because they can produce noise in data. To do so, and after evaluating any
171 capture anomaly, images were cut again to 325 pixels, which was the diameter of the Petri
172 dish whose surface was completely covered by the sample. Once this was done, images
173 were decomposed into three, each containing only the information from one of the red,
174 green or blue channels. Colour channels were split to collect information from not only
175 the R pixels, but also from G and B. In this case, the used wavelength stimulated pixels
176 from all the channels. This is done because the laser excites the G and B sensor, although
177 with less efficiency (Batistell et al., 2014), allowing us to get valuable information from
178 the R saturated areas with one single capture. The camera sensor quantize R, G and B
179 values with only 8 bits, thus if a big difference in light intensity exists in the scene, the
180 limited dynamic range cannot accurately represent all the nuances. Taking advantage of
181 the different efficiency of sensors we can recover part of this information. The last step
182 involved transforming images into data (descriptors that express the spatial intensity
183 signal). To this end, segmentation was done, where the different tones of the laser-pattern
184 morphology for each channel, which went from 0 (darker colour) to 255 (brighter colour),
185 were delimited by different tone intensities and measured as number of pixels. The free
186 FIJI image software was used to process all the images.

187 Two different groups of descriptors were generated; relative and direct descriptors.
188 Specific software was developed to automatically process and extract descriptors from
189 images, which was used in another study (Verdu et al., 2019a). To obtain the former, a
190 line of 325 pixels to cross the images in the center (the dashed yellow line in Fig. 1C) was
191 selected. From this, a profile was generated by the tone of each pixel that expresses the
192 intensity signal. Finally, descriptors were obtained with the number of pixels of the tone
193 located at 20% (w4), 40% (w3), 60% (w2), 80% (w1) and 100% (w0) of the maximum
194 tone value (w Max).

195 To obtain the direct descriptors (Fig. 1D), images were segmented between two intensities
196 (values of tones (0 to 255)), and the number of pixels between both values was defined
197 as a direct descriptor. So six direct descriptors were defined according to the established
198 tone interval: A250 (tone 250 to 151), A150 (tone 150 to 101); A100 (tone 100 to 76);
199 A75 (tone 75 to 51); A50 (tone 50 to 36); A35 (tone 35 to 0).

200

201 2.2.4. Statistical analyses

202 Factors enzyme treatment, enzyme action time and cooking process were studied by a
203 multifactor analysis of variance for the physico-chemical properties data and the principal
204 component analysis (PCA) values. In those cases with a significant effect ($p<0.05$), the
205 average was compared by Fisher's least significant difference (LSD). The PCA was used
206 to reduce image analysis data dimensionality to perform a joint comparative analysis.
207 Support vector machine (SVM) for regression (SVM-R) was applied to study the
208 dependency between the texture data and image data by evaluating the calibration (R^2)
209 and crossvalidation (R^2 CV) coefficients and the root mean square errors (RMSE). SVM
210 is a supervised learning methodology based on the statistical learning theory, which is

211 frequently used for spectral data analyses (Boser et al., 1992). Procedures were performed
212 with the PLS Toolbox 6.3 (Eigenvector Research Inc., Wenatchee, Washington, USA), a
213 toolbox extension in the Matlab 7.6 computational environment (The Mathworks, Natick,
214 Massachusetts, USA).

215

216 **3. Results and Discussion**

217 3.1. Physico-chemical properties

218 The three evaluated factors (enzyme treatment, enzyme action time and cooking methods)
219 statistically influenced both the texture and mass variation of pork loins. Figure 2A shows
220 the shear force values for the control and treated samples before and after cooking.
221 Enzyme treatment reduced the shear force, which became more evident when the enzyme
222 action time prolonged. While the shear force values slightly rose with the control samples
223 during the study, with statistically significant differences being found only for samples at
224 0 and 24 h and after cooking, the values of the samples treated with papain lowered.
225 Values mainly lowered during the first 6 h, from which point the shear force values did
226 not change until the end. Papain is a highly efficient enzyme that causes significant
227 degradation of both myofibrillar and collagen proteins (Ashie et al., 2002a) by the
228 specificity action on amino acids with aromatic side chains, such as Phe (Phenylalanine)
229 and Tyr (Tyrosine), at the P2 position (Singh et al., 2018).

230 The increased shear force values for the control samples could be due to the water lost
231 during this period (Fig. 2B). Water loss from whole raw meat can take place through the
232 action of endogenous proteolytic enzymes (calpains, cathepsins, caspases) as exudation,
233 and by water evaporation from the surface when muscle is cut (Tornberg, 2005).
234 Proteolytic enzymes are responsible for muscle fibre degradation (Bhat et al., 2018)

because myofibrils hold water (≈ 80%) in the spaces between thick and thin filaments in living muscle (Offer et al., 1989). During this action, which is called tenderness, endogenous proteolytic enzymes, mainly μ-calpain (Bhat et al., 2018), in muscle break up the myofibril structure and tenderise meat (Morton et al., 2018), losing water. As the control samples did not undergo softening, but quite the opposite, hardening, we expected water loss to be due to evaporation. In fact meat drying promotes closer contact between proteins and new interactions form that increase hardness (Aliño et al., 2009).

However, the papain-treated samples underwent the same water loss as the control during the first 6 h, which was lower at the end of the experiment (Fig. 2B). According to the results reported by other authors (Ashie et al., 2002b; Eom et al., 2015; Takei et al., 2015), the marked papain activity on the protein structure produced a rapid and strong hydrolytic effect on connective tissues by breaking polypeptides (Barekat and Soltanizadeh, 2017), which minimized water loss at the end of the experiment and increased softness. In fact, Figure 3 shows the augmented image of the treated and control samples at the 24-hour enzyme action time, where the hydrolytic effect is visible mainly on connective tissues (letter "c" in Fig. 3A). Instead the control samples showed superficial dark grooves (letter "d" in Fig. 3B) because of the hole generated by water loss. Both these behaviours became more evident when images were analyzed. For this purpose, images were transformed into the greyscale from 0 (black) to 255 (white), and a line of pixels was evaluated. The line of pixels showed heterogeneous tone values in the control sample (the purple line in Fig. 3), which were homogeneous for the treated sample (the blue line in Fig. 3) because hydrogel formed on the surface. Langmuir and Schaefer already reported papain's ability to form gel as a monolayer back in 1939, which could form on the surface of samples. This could explain why enzyme action finished 6 h after it was applied. Gel formation can lead to enzyme immobilization and, therefore, to its action.

The effect of cooking brought about increased hardness for both sample types and for all the enzyme action times (Fig. 2A), compared to the uncooked samples. During heating, the different meat proteins denature and cause structural changes in meat, such as the destruction of cell membranes, shrinkage of meat fibres, the aggregation and gel formation of myofibrilar and sarcoplasmic proteins, and shrinkage and solubilisation of connective tissue (Tornberg, 2005). Specifically at 80 ºC, hardness increases (Becker et al., 2016) due to denaturation of myofibrillar protein, which predominate in *Longissumus lumborum* (Walsh et al., 2010). This denaturation also caused water loss, which was around 25% for both sample types (Fig. 2B). Even so, the treated samples displayed a sharp drop in hardness compared to the untreated ones, with values close to those of the uncooked treated samples. This result was clearly observed with the samples that underwent enzyme treatment for 6 h at 4 ºC and were then cooked (Fig. 2A). A rise in temperature during cooking could enhance enzyme action. In fact papain's optimal activity occurs at temperatures within the 65-80 ºC range (Barekat and Soltanizadeh, 2017; Singh et al., 2018). Thus increasing temperature during cooking accelerates enzyme activity of myofibrillar proteins, which was so high that it minimised their shrinkage due to cooking, and also diminished their water-holding capacity and, therefore, increased water loss. This effect was clearly observed at enzyme action time 0 (Fig. 2A). At this time, the enzyme was added to samples and they were immediately cooked at the same time as the untreated samples, but shear force was much lower for the former. So a low cooking temperature with an effect on enzyme action (from 65 ºC) and the cooking method (e.g. stewing) could make the softness values of the meat treated with papain rise, as herein demonstrated. This cooking process would have the main advantage (meat tenderness) of low-temperature long-time cooking (LTLT), but without its disadvantages (juiciness and cooking loss) (Dominguez-Hernandez et al., 2018).

285 3.2. Image analysis

286 Having processed the images before cooking and generated the descriptors for each
287 channel, data were explored following the differences observed in the space of variance
288 obtained in the PCA. Four components expressed 77.75% of variance, being PC1 with
289 43.78% which could be related to sample type (with or without enzyme treatment) and
290 enzyme action time. When the weights of each descriptor (loadings) on the PCA were
291 analyzed (Fig. 4A), the Green channel descriptors were the most influential, followed by
292 those of the Blue channel. For both, the relative descriptors (W) had more descriptors
293 with higher loading values than the direct descriptors (A), perhaps because they depend
294 less on sample thickness. Instead the Red channel had the fewest descriptors with high
295 weight values (only W2 and W3). As the laser emitted light at 650 nm (red), the Red
296 channel was expected to be the most influential on the generated PCA model. One
297 explanation could lie in the web cam characteristics. The three sensors (red, green, blue)
298 are sensitive to a wavelength range (spectrum) and, therefore, to 650 nm at different levels
299 (red sensor was the most excited, while green and blue were less excited). So Red channel
300 sensors could be saturated and samples change because of factors (enzyme treatment and
301 enzyme action time), which would not suffice to reduce saturation or, if reducing it, some
302 information could be lost. This could explain the highest values of the descriptors for this
303 channel. Instead for the Green and Blue channels, although the excitation of sensors was
304 lower, the changes in samples would generate changes on the laser patterns, and they
305 would suffice to change sensor excitation and, consequently, the generated descriptors.

306 So, by employing only the descriptors with a high weight value in the PCA (the
307 descriptors inside the dashed black line box in Fig. 3A), a new PCA study was performed.
308 In this case, the results improved as total variance rose to 98.14% and PC1 component
309 had 89.02% of the total. Figure 3B shows the representation of the PC1 values during the

310 enzyme action time. PC1 evolution was dependent on the enzyme action time, with the
311 same behaviour displayed by both sample types. The PC1 values lowered with time, being
312 lower for the papain-treated samples, which reached the lowest PC1 value (maximum
313 difference) at the 6-hour treatment time, like that observed for shear force and mass loss
314 (Fig. 2). The PC1 result was clearly understood when the descriptors with the highest
315 weight values in the PCA model were observed. Figure 5A, by way of example, shows
316 the evolution on descriptor W2 for the three channels. For both sample types, the
317 descriptor values lowered, as with the other descriptors, which could reveal the reduction
318 of light through samples. During the study, both sample types lost water, which increased
319 the contact between proteins, as previously mentioned, and less light crossed samples. In
320 addition, for the treated samples, this reduction could be done mainly to the disruption of
321 the protein structure, the delocated water content and gel formation, which would all
322 generate an amorphous structure like that shown in Figure 3A. In this disordered structure,
323 the Anderson localisation phenomenon would take place (Wiersma et al., 1997). Based
324 on this phenomenon, light diffusion in a disordered system might come to a halt
325 (confined) when disorder reaches a critical value. The scattering process carried out due
326 to the marked disorder caused the material to reduce the light transmitted through it by
327 exponentially reducing the transmission coefficient with sample thickness (Wiersma et
328 al., 1997), which can become opaque.

329 The study of the images obtained from the samples after cooking was conducted as
330 previously for the samples before it. The PCA generated by employing descriptors did
331 not show any relation with both factors (enzyme action time and cooking process). The
332 evaluation of the descriptors from Green and Blue channels displayed chaotic behaviour,
333 which was instead coherent for the Red channel. In line with this result, a new PCA was
334 done by employing only the descriptors of the Red channel. The new model was obtained

by employing five components, which expressed 97.05% of the total variance, while PC2 explained 22.21% of the total variance, which was related to both factors. The analysis of the loading showed that descriptors W2, W3, W3/W0, W3/W1, A75, A50 and A35 had the highest weight values in the PCA model (Fig. 4C). So a third PCA analysis was done and used only these descriptors. In this new PCA, only two components were needed (83.57%), and PC1 explained 46.66%, of the total variance, which was related to both factors. Figure 4D shows the evolution of the PC1 values during the enzyme action time. The evolution of the PC1 values differed from both sample types. While no evolutions and only moderate increases were observed for the control samples, for the treated samples abrupt decreases took place during the first 6 h, which remained constant after this period. Evolution was similar to that observed for texture and water loss after cooking (Fig. 2A and B). The main factor affecting samples was the cooking process. On the one hand, it lowered the descriptors' values, compared to those obtained for the uncooked samples (Fig. 5A and B); on the other hand, it enhanced enzyme action, as previously mentioned. The lower descriptors' values were because cooking led to the shrinkage and compaction of meat fibres, which hindered the laser light from passing through samples, as shown in Fig. 1C and 1D. In them, the laser pattern of both samples is shown and the smaller diameter for samples with cooking treatment is clearly observed. This result could explain why the highest weight values in the PCA model were given only by the descriptors from the Red channel. The smallest amount of light to pass through samples would not be enough to excite the sensors of the Green and Blue channels and as a result, descriptors with chaotic behaviour. Besides, the increase in enzyme action brought about by the cooking process, as seen in the shear force study (Fig. 2A), was clearly observed at enzyme action time 0. At this time point, the values of descriptors and PC1 (Fig. 5B and 4D, respectively) were much lower in the treated samples. The disruption of the

360 protein structure, gel coagulation and, therefore, the generated amorphous structure
361 would increase samples' opacity, possibly because of the increased Anderson localisation
362 phenomenon.

363

364 3.3. Relation between physico-chemical and image results

365 After observing the same behaviour among water loss, shear force and the changes in the
366 laser-backscattering imaging, the relation among those in which changes were evident
367 was evaluated for each one. For changes in the laser-backscattering imaging, PC1 was
368 uses as result of the linear combinations of image descriptors to one variable. Figure 6A
369 shows the relation among the mass loss for untreated and treated uncooked samples, for
370 the treated and cooked samples, and their respective PC1 values. Figure 6B depicts the
371 shear force relation for the uncooked treated and the treated + cooked samples and their
372 respective PC1 values. For the uncooked samples, although the untreated samples
373 displayed greater mass loss, changes in the PC1 values were higher for the treated
374 samples, which revealed the importance of the protein structure disruption generated by
375 enzymatic activity on the laser response, as evidenced by the observed relation between
376 shear force and PC1 (Fig. 6B). Thus, for the uncooked samples, changes in laser pattern
377 would occur by the dehydration, while these would vastly increase by the changes in
378 texture caused by the enzyme in the treated samples.

379 For the cooked samples, although a relation appeared between mass loss and PC1 for the
380 treated samples (Fig. 6A), as there was no significant variation in it, the changes in PC1
381 should be attributed mainly to texture changes (see Fig. 6B).

382 One relation was evaluated, support vector machine for regression (SVM-R) was applied
383 to study the dependence among mass loss, texture and images for those treatments with

384 changes. The results did not show any model between mass loss and image changes,
385 regardless of treatment. Although a relation was found (Fig. 6A), data dispersion made it
386 impossible to develop any model. Instead three models were constructed between the
387 texture and images of the samples treated with the enzyme: one employed the uncooked
388 samples, another used the cooked samples and the third utilised both. Table 1 shows the
389 prediction results. The obtained R^2 were higher than 0.90 for all the models, and no
390 differences in errors were specifically observed. The goodness of the obtained models
391 was evident when the average of the standard error for texture (in Table 1 of
392 Supplementary Material), which expresses the variability in meat texture at each sampling
393 time, was compared to the RMSE values for the models (Table 1), which express the error
394 in texture prediction. While the average for the former was 2.9 and 2.6 for the uncooked
395 and cooked samples, respectively, the highest RMSE was 1.902. So the obtained models
396 could confirm the direct relation between meat structure (independently of the cooking
397 process) and the laser pattern generated when structure changes sufficed to minimise
398 other effects, such as drying, which occurred with the control samples before cooking.

399

400 **4. Conclusion**

401 The laser-backscattering imaging technique tool was proven capable of evaluating pork
402 loin tenderness based on three factors: enzyme pretreatment, enzyme action time, cooking
403 method.

404 Enzyme action increased sliced fresh pork loin tenderness and its maximum value was
405 obtained at 6 h of enzymatic treatment at 4ºC, but the cooking process considerably
406 increased activity because the temperature set (80ºC) fell within the optimal enzyme

activity temperatures range (65–80ºC). Activity is so high that it can minimise the marked increase in hardness due to cooking.

Changes in samples brought about changes in the image descriptors. For the samples before cooking, the descriptors from Green and Blue channels were the most influential, while the Red channel was for the samples after cooking. Samples' increased opacity due to water loss and compaction, mainly by cooking, led the Red channel to go from saturation to an adequate excitation level, while the Green and Blue channels went from a good excitation level to non-excitation. Hence decomposition of the images in the three channels (Red, Green, Blue) allows us to analyse the samples that undergo marked changes while being processed without varying the image capture system.

The relations between the changes in both laser pattern and meat texture caused by the enzyme, and independently of the cooking method, were demonstrated whenever enzymatic changes minimised other effects like drying. So this technique could be used to evaluate meat texture by reducing the effect that meat heterogeneity has on the mean texture value obtained by employing destructive techniques such as texturometers.

Acknowledgments

The authors thank the "Ministerio Español de Ciencia e Innovación" for the financial support provided through Project RTI2018-098842-B-I00.

References

Aliño, M., Grau, R., Baigts, D., Barat, J.M., 2009. Influence of sodium replacement on the salting kinetics of pork loin. J. Food Eng. 95, 551-557. https://doi.org/10.1016/j.jfoodeng.2009.06.016

Ashie, I. N. A., Sorensen, T. L., & Nielsen, P. M. 2002a. Effects of Papain and a Microbial Enzyme. Food Chem. Toxicol., 67(6), 2138–2142.

Ashie, I.N.A., Sorensen, T.L., Nielsen, P.M., 2002b. Effects of Papain and a Microbial Enzyme on Meat Proteins and Beef Tenderness. J. Food Sci. 67, 2138–2142. https://doi.org/10.1111/j.1365-2621.2002.tb09516.x

Barekat, S., Soltanizadeh, N., 2017. Improvement of meat tenderness by simultaneous application of high-intensity ultrasonic radiation and papain treatment. Innov. Food Sci. Emerg. Technol. 39, 223–229. https://doi.org/10.1016/j.ifset.2016.12.009

Batistell, G., Zhang, V. C., & Sturm, J., 2014. Color recognition sensor in standard CMOS technology. Solid-State Electronics, 102, 59–68. https://doi.org/10.1016/j.sse.2014.06.002

Becker, A., Boulaaba, A., Pingen, S., Krischek, C., & Klein, G. 2016. Low temperature cooking of pork meat - Physicochemical and sensory aspects. Meat Sci., 118, 82–88. https://doi.org/10.1016/j.meatsci.2016.03.026

Bhat, Z.F., Morton, J.D., Mason, S.L., Bekhit, A.E.D.A., 2018. Role of calpain system in meat tenderness: A review. Food Sci. Hum. Wellness 7, 196–204. https://doi.org/10.1016/j.fshw.2018.08.002

Bolumar, T., Bindrich, U., Toepfl, S., Toldrá, F., Heinz, V., 2014. Effect of electrohydraulic shockwave treatment on tenderness, muscle cathepsin and peptidase activities and microstructure of beef loin steaks from Holstein young bulls. Meat Sci. 98, 759–765. https://doi.org/10.1016/j.meatsci.2014.07.024

Boser, E., Vapnik, N., Guyon, I.MT.B. Laboratories. 1992. Training algorithm margin for optimal classifiers. Perception, 144-152.

Dominguez-Hernandez, E., Salaseviciene, A., & Ertbjerg, P. 2018. Low-temperature long-time cooking of meat: Eating quality and underlying mechanisms. In Meat Sci. 143, 104–113. https://doi.org/10.1016/j.meatsci.2018.04.032

455 Eom, S.H., Lee, S.H., Chun, Y.G., Kim, B.K., Park, D.J., 2015. Texture softening of beef and
456 chicken by enzyme injection process. Korean J. Food Sci. Anim. Resour. 35, 486–493.
457 https://doi.org/10.5851/kosfa.2015.35.4.486

458 Langmuir, I., & Schaefer, V. J., 1939. Properties and structure of protein monolayers. Chem.
459 Rev., 24(2), 181–202. https://doi.org/10.1021/cr60078a002

460 Lomiwes, D., Farouk, M.M., Wiklund, E., Young, O.A., 2014. Small heat shock proteins and
461 their role in meat tenderness: A review. Meat Sci. 96, 26–40.
462 https://doi.org/10.1016/j.meatsci.2013.06.008

463 Mollazade, K., Omid, M., Akhlaghian Tab, F., Kalaj, Y. R., Mohtasebi, S. S., & Zude, M.,
464 2013. Analysis of texture-based features for predicting mechanical properties of
465 horticultural products by laser light backscattering imaging. Comput. Electron. Agric.,
466 *98*, 34–45. https://doi.org/10.1016/j.compag.2013.07.011

467 Morton, J.D., Bhat, Z.F., Bekhit, A. E.-D. A., 2018. Proteases and meat tenderization, in:
468 Encyclopedia of Food Chemistry. Elsevier, pp. 309–313. https://doi.org/10.1016/B978-0-
469 08-100596-5.21663-6

470 Offer, G., Knight, P., Jeacocke, R., Almond, R., Cousins, T., Elsey, J., Parsons, N., Sharp, A.,
471 Starr, R., Purslow, P., 1989. The structural basis of the water-holding, appearance and
472 toughness of meat and meat products. Food Microstruct. 8, 151–170.

473 Bruce, H. L., & Aalhus, J. L. 2017. Advances in the Understanding and Measurement of Meat
474 Texture. In New Aspects of Meat Quality. https://doi.org/10.1016/b978-0-08-100593-
475 4.00008-4

476 Silva, D.R.G., Torres Filho, R.A., Cazedey, H.P., Fontes, P.R., Ramos, A.L.S., Ramos, E.M.,
477 2015. Comparison of Warner-Bratzler shear force values between round and square cross-
478 section cores from cooked beef and pork Longissimus muscle. Meat Sci. 103, 1–6.
479 https://doi.org/10.1016/j.meatsci.2014.12.009

480 Singh, P.K., Shrivastava, N., Ojha, B.K., 2018. Enzymes in the meat industry. Enzym. Food
481 Biotechnol. Prod. Appl. Futur. Prospect. 111–128. https://doi.org/10.1016/B978-0-12-
482 813280-7.00008-6

483 Taheri-Garavand, A., Fatahi, S., Omid, M., Makino, Y., 2019. Meat quality evaluation based on
484 computer vision technique: A review. Meat Sci. 156, 183–195.
485 https://doi.org/10.1016/j.meatsci.2019.06.002

486 Takei, R., Hayashi, M., Umene, S., Narita, K., Kobayashi, Y., Masunaga, H., 2015. Changes in
487 Physical Properties of Enzyme-Treated Beef Before and After Mastication. J. Texture
488 Stud. 46, 3–11. https://doi.org/10.1111/jtxs.12103

489 Talens, P., Castells, M.L., Verdú, S., Barat, J.M., Grau, R., 2021. Flow, viscoelastic and
490 masticatory properties of tailor made thickened pea cream for people with swallowing
491 problems. J. Food Eng. 292, 260–8774. https://doi.org/10.1016/j.jfoodeng.2020.110265

492 Toldrá, F., 2012. Biochemistry of Processing Meat and Poultry, in: Food Biochemistry and
493 Food Processing: Second Edition. Wiley-Blackwell, pp. 303–316.
494 https://doi.org/10.1002/9781118308035.ch16

495 Toldrá, F., Reig, M., 2015. Enzymes in meat and fish, in: Improving and Tailoring Enzymes for
496 Food Quality and Functionality. Elsevier Inc., pp. 199–212. https://doi.org/10.1016/B978-
497 1-78242-285-3.00010-7

498 Tornberg, E., 2005. Effects of heat on meat proteins - Implications on structure and quality of
499 meat products, in: Meat Sci. Elsevier Ltd, pp. 493–508.
500 https://doi.org/10.1016/j.meatsci.2004.11.021

501 Tu, K., Jancsók, P., Nicolaï, B., De Baerdemaeker, J., 2000. Use of laser-scattering imaging to
502 study tomato-fruit quality in relation to acoustic and compression measurements. Int. J.
503 Food Sci. Technol. 35, 503–510. https://doi.org/10.1046/j.1365-2621.2000.00407.x

504 Udomkun, P., Nagle, M., Mahayothee, B., & Müller, J. 2014. Laser-based imaging system for

505 non-invasive monitoring of quality changes of papaya during drying. Food Cont., 42, 225–
506 233. https://doi.org/10.1016/j.foodcont.2014.02.010

507 Verdú, S., Barat, J.M., Grau, R., 2019a. Laser backscattering imaging as a non-destructive
508 quality control technique for solid food matrices: Modelling the fibre enrichment effects
509 on the physico-chemical and sensory properties of biscuits. Food Cont. 100, 278-286.
510 https://doi.org/10.1016/j.foodcont.2019.02.004

511 Verdú, S., Barat, J.M., Grau, R., 2019b. Non destructive monitoring of the yoghurt fermentation
512 phase by an image analysis of laser-diffraction patterns: Characterization of cow's, goat's
513 and sheep's milk. Food Chem. 274, 46-54.
514 https://doi.org/10.1016/j.foodchem.2018.08.091

515 Verdú, S., Pérez, A.J., Barat, J.M., Grau, R., 2020. Non-destructive control in cheese
516 processing: Modelling texture evolution in the milk curdling phase by laser backscattering
517 imaging. Food Cont. 107638. https://doi.org/10.1016/j.foodcont.2020.107638

518 Verdú, S., Pérez, A.J., Barat, J.M., Grau, R., 2019c. Laser backscattering imaging as a control
519 technique for fluid foods: Application to vegetable-based creams processing. J. Food Eng.
520 241, 58-66. https://doi.org/10.1016/j.jfoodeng.2018.08.003

521 Walsh, H., Martins, S., O' Neill, E.E., Kerry, J.P., Kenny, T., Ward, P., 2010. The effects of
522 different cooking regimes on the cook yield and tenderness of non-injected and injection
523 enhanced forequarter beef muscles. Meat Sci. 84, 444–448.
524 https://doi.org/10.1016/j.meatsci.2009.09.014

525 Wiersma, D.S., Bartolini, P., Lagendijk, A., Righini, R., 1997. Localization of light in a
526 disordered medium. Nature 390, 671–673. https://doi.org/10.1038/37757

527

Figure 1

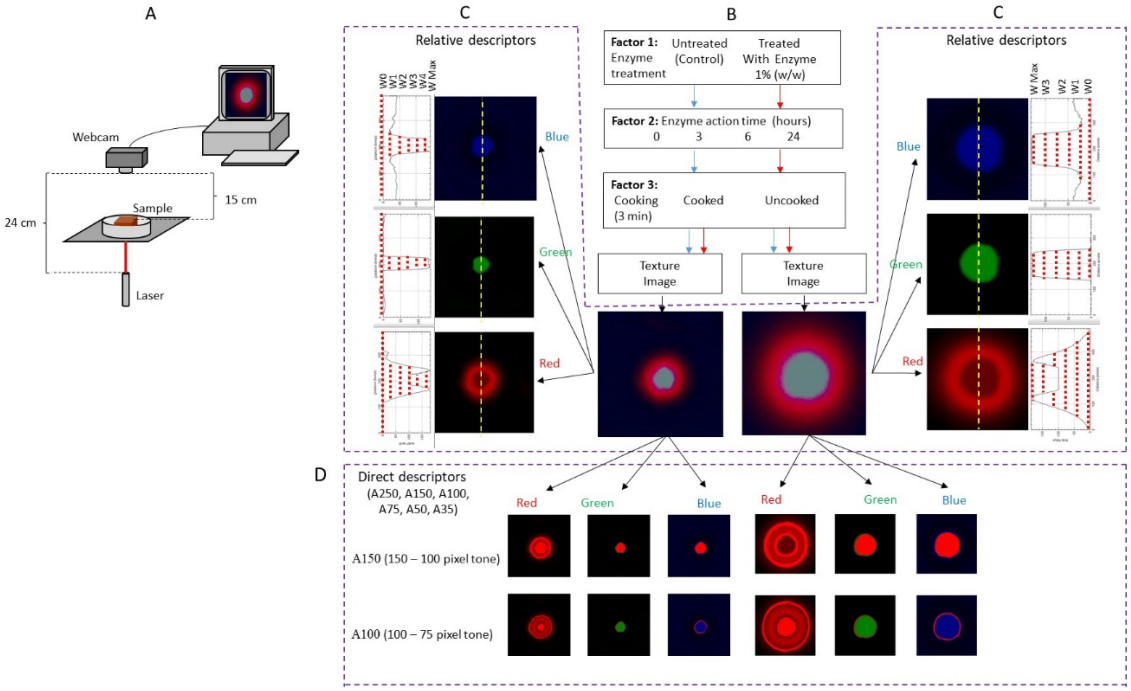

Fig. 1. A: Image device scheme; B: Scheme of the experiment; C and D: Image processing and data extraction by decomposing the RGB images into those with information from the Red, Green and Blue channels to obtain relative descriptors (C) and direct descriptors (D).

538 Figure 2

539

540

541

542

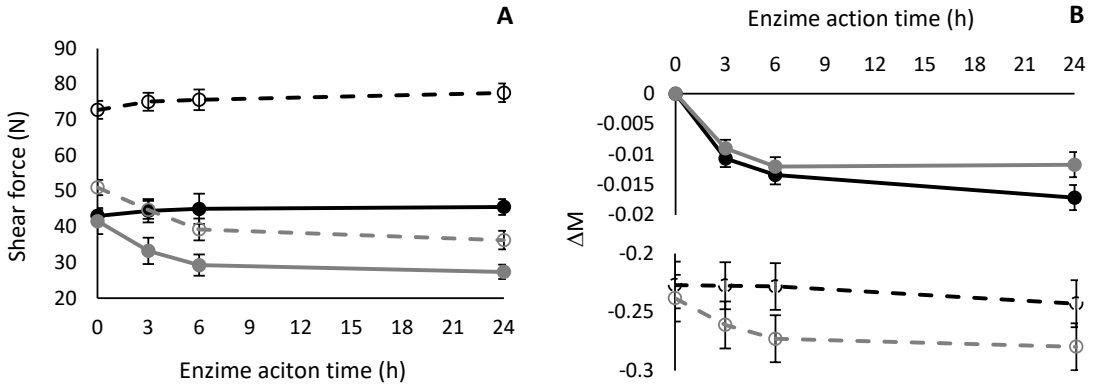

543

544

545 Fig. 2. Texture (A) and mass variation (B) for the control (black line) and treated samples
546 (grey line) for each enzyme action time. Continuous line: uncooked samples. Dashed line:
547 cooked samples. Bars represent standard deviation.

548

549 Figure 3

550

551

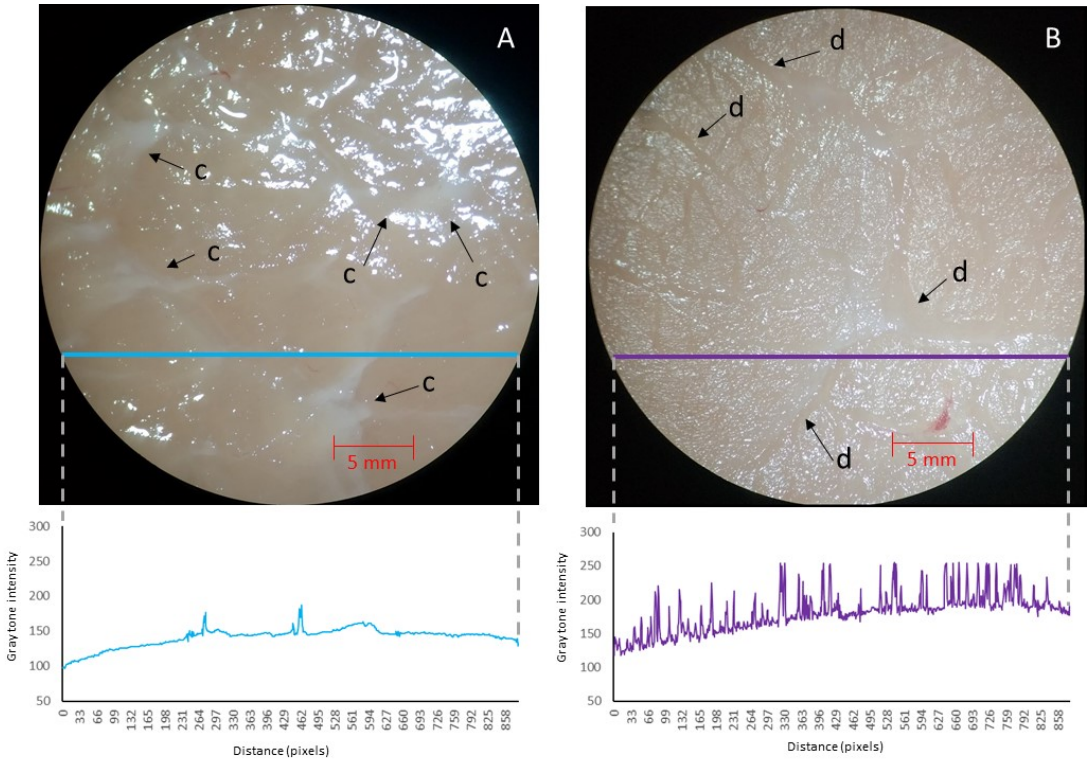

552

553 Fig. 3. Augmented image of the treated (A) and control (B) samples at enzyme action
554 time 24 h. c: hydrolytic effect on connective tissues; d: dark grooves by water loss. Blue
555 and purple line: line of pixels in which the gray tone was analyzed. Graphs: gray tone
556 intensity at each pixel.

557

Figure 4

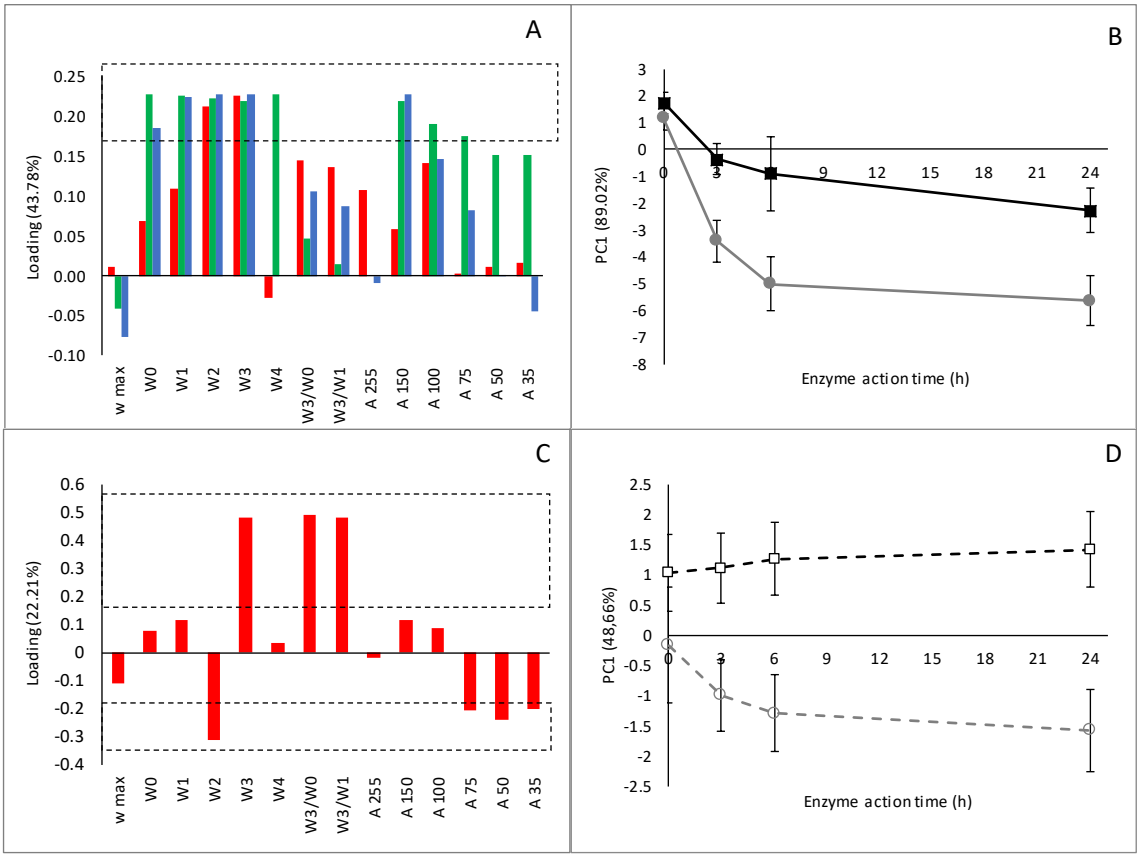

Fig. 4. A: Loading for the first PCA analysis done with the descriptors obtained from the three channels of images of the uncooked samples. B: PCA done only with the descriptors with higher weight values on the first PCA. C: Loading for the second PCA analysis done with the descriptors obtained from the Red channels of images of the cooked samples. D: PCA done only with the descriptors with higher weight values on the second PCA. Red line: Red channel; Green line: Green channel; Blue line: Blue channel; Black line: control uncooked samples; Grey line: treated uncooked samples; Black dashed line: control cooked samples; Grey dashed line: treated cooked samples; Dashed black line box: the descriptors considered with high weight values in the PCA model. Bars represent standard deviation.

573 Figure 5

574

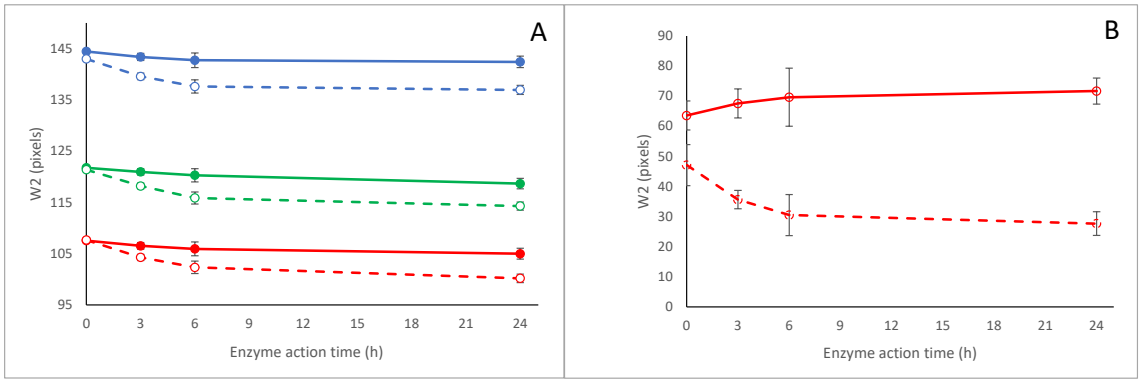

575

576 Fig. 5. Evolution of descriptor W2 for the Red, Green and Blue channels for the uncooked
577 samples (A) and Red channel for the cooked samples (B). Red line: Red channel; Green
578 line: Green channel; Blue line: Blue channel. Bars represent standard deviation.

579

580 Figure 6

581

582

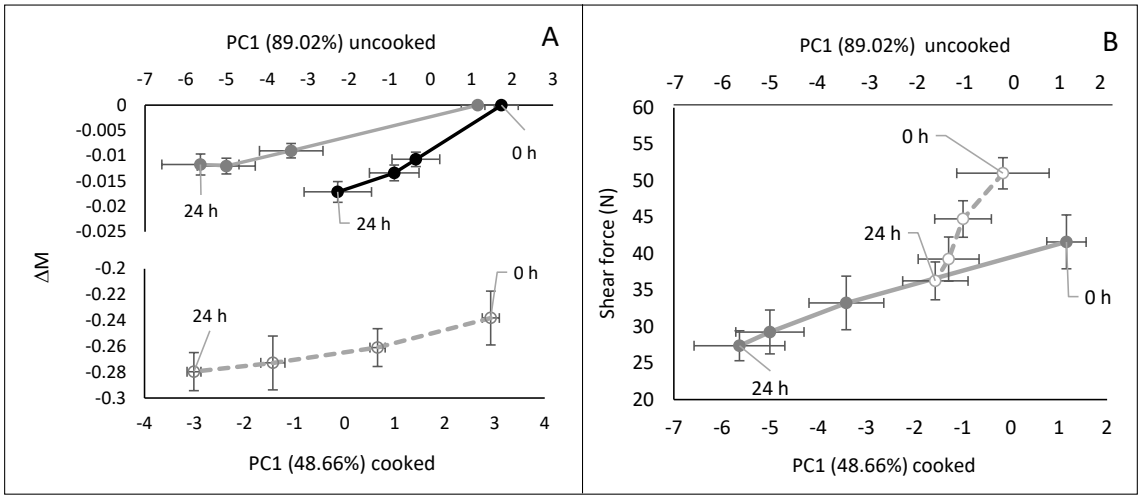

583

584 Fig. 6: Relation between the mass loss (A) or shear force (B) with the PC1 obtained from
585 PCA analysis of the image descriptors. Continuous black line: untreated and uncooked
586 samples; Continuous gray line: treated and uncooked samples; Dashed gray line: treated
587 and cooked samples. Bars represent standard deviation.

588

589 Table 1

590

591 Table 1. Prediction parameters for the regression models between the shear force and

592 imaging data of the treated samples.

593

Model performance

	uncooked	cooked	uncooked + cooked
RMSE C	1.394	0.564	1.217
RMSE CV	1.704	1.403	1.902
Bias C	0.2867	0.0547	0.0957
Bias CV	0.3497	0.2671	0.07012
R^2 C	0.945	0.989	0.962
R^2 CV	0.916	0.923	0.904

594

595

596